Published in final edited form as:
NMR Biomed. 2013 October ; 26(10): 1271–1277. doi:10.1002/nbm.2947.

Amide Proton Transfer Imaging of the Human Breast at 7 Tesla: Development and Reproducibility

Dennis W. J. Klomp[1,2], **Adrienne N. Dula**[2,3], **Lori R. Arlinghaus**[2], **Michel Italiaander**[1], **Richard D. Dortch**[2,3], **Zhongliang Zu**[2], **Jason M. Williams**[2,3], **Daniel F. Gochberg**[2], **Peter R. Luijten**[1], **John C. Gore**[2,3,4,5,6], **Thomas E. Yankeelov**[2,3,4,6,7], and **Seth A. Smith**[2,3,4,6]

[1]Department of Radiology, University Medical Center Utrecht, Utrecht, the Netherlands [2]Institute of Imaging Science, Vanderbilt, Nashville, USA [3]Department of Radiology and Radiological Sciences, Vanderbilt, Nashville, USA [4]Department of Biomedical Engineering, Vanderbilt, Nashville, USA [5]Department of Molecular Physiology and Biophysics, Vanderbilt, Nashville, USA [6]Department of Physics, Vanderbilt, Nashville, USA [7]Department of Cancer Biology, Vanderbilt, Nashville, USA

Abstract

Chemical exchange saturation transfer (CEST) can offer information about protons associated with mobile proteins through the amide proton transfer (APT) effect, which has been shown to discriminate tumor from healthy tissue and, more recently, has been suggested as a prognosticator of response to therapy. Despite this promise, APT effects are small (only a few percent of the total signal); and APT imaging is often prone to artifacts resulting from system instability. Here we present a procedure that enables the detection of APT effects in the human breast at 7 T while mitigating these issues. Adequate signal-to-noise ratio (SNR) was achieved *via* an optimized quadrature RF breast coil and 3D acquisitions. To reduce the influence of fat, effective fat suppression schemes were developed that did not degrade SNR. To reduce the levels of ghosting artifacts, dummy scans have been integrated into the scanning protocol. Compared to results obtained at 3 T, the standard deviation of the measured APT effect was reduced by a factor of four at 7 T, allowing for the detection of APT effects with a standard deviation of 1% in the human breast at 7 T. Together, these results demonstrate that the APT effect can be reliably detected in the healthy human breast with a high level of precision at 7 T.

Keywords

CEST; APT; breast; 7 T

Introduction

Sensitive and specific imaging biomarkers are required for accurate diagnosis, evaluation of therapeutic intervention, and monitoring of disease progression. An increase in the sensitivity and specificity of imaging biomarkers has the potential to improve patient care. MRI, owing to its flexibility for generating multiple contrasts within one set of imaging experiments, has developed into one of the primary imaging techniques for assessing human disease. While flexible and sensitive to certain pathologies, MRI is often non-specific for the substrates of pathology.

Dennis W. J. Klomp, Address of corresponding author: University Medical Center Utrecht, Department of Radiology, PO Box 85500 3508 GA Utrecht, The Netherlands Tel: +31 88 7551391, D.W.J.Klomp-2@umcutrecht.nl.

Chemical exchange saturation transfer (CEST) seeks to indirectly observe the exchange of specific labile protons that are generally not detectable with standard MRI methods. As such, CEST imaging may provide a more specific means to probe tissue composition compared to conventional MRI. Unfortunately, the sensitivity of the MRI signal to these protons can be quite low, especially at lower field strengths. High field CEST imaging offers increased signal-to-noise ratio (SNR), increased spectral dispersion, and increased saturation survival for a given power due to the prolongation of T_1 with field strength; therefore, there is a great deal of interest in developing CEST imaging at high field to overcome the aforementioned sensitivity issues.

CEST MRI is unique in that it has the ability to assess amide protons of mobile proteins/peptides [1] and hydroxyl moieties found in glycogen [2] and has recently been reported to be sensitive to exchangeable protons found in GAG [3], glutamate [4], myoinositol [5], and creatine [6]. Specifically, when considering the CEST effect that arises from protons associated with the amide bond in proteins and peptides (so-called amide proton transfer or APT), significant changes in the CEST effect have been reported in brain tumors [7] and ischemic tissue resulting from stroke [8] when compared to healthy tissue [1]. Likewise, Dula *et al.* [9] have shown that CEST MRI of the breast can anecdotally be related to treatment response in patients with breast cancer after neoadjuvant chemotherapy. Lastly, recent studies have shown the improvements in APT imaging that can be obtained at higher field strengths [10-12], along with sensitivity to other exchange mechanisms, such as the nuclear Overhauser effect (NOE) [10]; but to date, no studies have explored APT imaging of the human breast *in vivo* at 7 T.

With a reported effect size of a few percent of the entire signal [1-11], SNR and signal stability are crucial to any CEST measurement. Whole-body commercial MR systems have evolved up to a B_0 field strength of 7 T, which currently provides the highest theoretical SNR available for *in vivo* human studies (i.e. intrinsic SNR is linearly related to B_0). In fact, recent reports have shown excellent CEST results can be obtained in the human brain at 7 T [4-6, 10, 11], as both SNR is high and physiologic effects due to (for example) breathing, are sufficiently small [13]. In addition, stronger effects have been reported in brain tumors compared to healthy tissue with APT-CEST, thereby encouraging application of this technique to cancer. Unfortunately, while physiologically-induced image instabilities are minimal in the human brain [13], they can be substantial in body imaging, thus confounding the ability to sensitively characterize the CEST effect. In particular, respiratory and cardiac motion can produce up to 0.3 ppm of dynamic field distortions [14] in the human breast causing more rapid dephasing of spins at higher fields. At 3 T, APT-CEST effects of 5 ± 5% have been observed in the glandular tissue of the breast [9]; however, at higher field strengths the impact of physiological motions are likely more challenging to combat and this may counteract the increase in available SNR.

In this study, we demonstrate the first implementation of three-dimensional (3D) CEST imaging of the human breast at 7 T. A sensitivity-optimized RF coil dedicated for breast MRI at 7 T was used that resulted in a more than 5-fold gain in intrinsic signal sensitivity as compared to 3 T [15]. In addition, a fat-suppressed, short-TE steady-state acquisition was employed to maximize SNR and stability. The short TE minimizes spin dephasing as a consequence of changing susceptibility effects over time, which reduces ghosting artifacts. Likewise, the short TE maximizes SNR as T_2 relaxation will be minimal over this time. The fat suppression minimizes the signal intensities that will not provide a useful CEST effect, but could provide ghosting artifacts. The resulting preliminary 7 T CEST measurements (obtained in six healthy subjects) encourage the application of this technique in clinical breast cancer studies for potentially improving the sensitivity and specificity in both the diagnostic and prognostic setting.

Methods

A 7 Tesla whole-body MR system (Achieva, Philips Healthcare, Cleveland, USA) was used for all experiments. To ensure high SNR, a local transmit and receive quadrature breast coil was used. Coil elements were mounted directly on a cup designed to fit a single breast [16]. Subjects were positioned prone with their right breast in the cup. A dedicated mattress was designed that provided comfort and reduced motion artifacts. Six healthy female volunteers participated (age: 39 ± 14 years), and the study was approved by the local institutional review board.

Data Acquisition

CEST MRI acquisitions were obtained according to the following prescriptions. To ensure sufficient RF irradiation bandwidth to overcome effects of dynamic field fluctuations due to breathing, a train of RF pulses [7] was implemented rather than continuous wave irradiation for the CEST preparation. A total of 200 Gaussian-windowed one-lobe sinc RF pulses of 10 ms each were used at a nominal flip angle of 180° for each subpulse [17]. At an RF preparation duty-cycle of 50%, the irradiation duration was 4 s (200 repetitions of a 10ms on, 10ms off paradigm), which is approximately twice the T_1 relaxation of glandular tissue at 7 T (i.e., 2.3 s [18]) and therefore provides substantial saturation. RF irradiation was performed over 60 frequency steps: three at 1000 ppm offset from water (for normalization) and 57 frequency steps ranging from −5 ppm to +9 ppm in 0.25 ppm increments. In one subject, a *z*-spectrum was obtained with more sampling points (extending the range to +/−100 ppm, using a total of 128 frequency offsets) to investigate, apart from NOE, the affects of MT that contribute to z-spectrum in more detail.

Fat suppression was obtained using a water-selective, binominal RF excitation pulse train. The optimal inter-pulse distance for fat suppression at 7 T is 0.5 ms (i.e. $1/2\Delta\sigma_{WF}$,where $\Delta\sigma_{WF}$ is the difference in chemical shift between water and fat at 7 T); therefore, a 1-2-1 RF pulse was employed to allow for a short in-phase TE of 2 ms. The TR of the chosen turbo field echo (TFE) acquisition was set to a minimum value of 4 ms and the nominal excitation was set to the Ernst angle of 3.6° (based on the estimated T_1 for glandular tissue at 7 T [18]). With a slab selective excitation of 72 mm and a field of view of $(150\ mm)^2$, two 600 ms shots were needed to complete the 3D acquisition at a resolution of $3 \times 3 \times 6\ mm^3$. To minimize ghosting and blurring from the TFE readout, 30 startup excitations were applied before *k*-space acquisition, which was obtained *via* a center-out trajectory. Each frequency offset was performed in less than 10 s, resulting in an acceptable scan time of 5 minutes for the CEST measurement.

As the B_1 field of the breast coil is non-uniform, care was taken to ensure optimal SNR over all of the glandular tissue. The short TR of the readout train combined with the long T_1 of glandular tissue tended to equalize the SNR over the volume: By matching the flip angle to the Ernst angle within the area of the glandular tissue having the lowest B_1 (lowest sensitivity), the stronger B_1 (closer to the coil) will cause more spin saturation while acquired at higher sensitivity [19]. B_1^+ maps were obtained at a fixed RF peak power setting of 2.2 kW at the amplifier output for a nominal $B_{1\,max}^+$ of 30 μT using the actual flip angle imaging (AFI) method [20]. The RF power setting was adapted based on these maps for subsequent scans, using the flip angle setting to drive the B_1^+ level at the center of the breast until it matched the nominal angle. High-resolution MRI scans with minimized partial volume effects were obtained with fat suppression to measure the SNR from the glandular tissue and offer segmentation of glandular tissue. A fast field echo (FFE) was used with binominal 1-2-1 water selective excitation at a TE of 3 ms and a TR of 6.7 ms at a nominal flip angle of 10 degrees, which is approximately the actual Ernst angle at the lowest B_1^+ level in the glandular tissue of the breast.

Phantom measurements were obtained to investigate CEST spectral resolution, lipid suppression, and system stability. A tube with 3% agarose and 10 mM creatine at pH = 7.4 was positioned in a cup that contained fat (lard). Fat suppression performance was assessed by comparing the pixel intensities of the images obtained with the water-selective binominal pulse to the ones obtained with a conventional slab-selective excitation. Rather than obtaining spectra from an amide phantom, the CEST spectra of the creatine phantom demonstrated that our spectral resolution and power are more than sufficient to detect a narrow, faster exchanging amine lineshape at a an even smaller chemical shift ($\Delta\omega$ = 1.9 ppm). Finally, the ghosting strength was assessed to investigate system stability in the detection accuracy of CEST effects.

Data Analysis

The focus of the CEST experiments performed in this study was the amide proton resonance at 3.5 ppm. Thus, following the analysis methods presented in [9, 10], after normalization by the 1000 ppm acquisitions, we fit the CEST spectra as a function of offset frequency to a single Lorentzian. The minimum of this fitted Lorentzian was used as the center (water) frequency and voxel-wise spectra were shifted accordingly. Glandular tissue was then segmented, and the residuals between the glandular tissue CEST data and fitted Lorentzian were calculated. Note that successful fat suppression enabled application of a simple, threshold based segmentation. To characterize the CEST effect around the amide proton resonance, we averaged the residuals between the glandular CEST data and the Lorentzian fit over 3 to 4 ppm, and the averaged value was reported as a percentage of the non-saturated water signal (denoted herein as APT-CEST fraction). The mean and standard deviations of APT-CEST fractions were calculated for each subject. Finally, to compare with conventional asymmetry analysis, we also calculated the MTR_{asym} according to Zhou *et al.* [7].

Results

The B_1^+ field of the breast coil resembles a uniform field over the coronal slices, while substantially decaying in the anterior-posterior direction (Fig 1a). Over a 5 cm distance from anterior to posterior, the B_1^+ field decreases by 50% (Fig. 1b). At an RF power level of 1 kW, the minimum B_1^+ level in the phantom reaches 60% of the nominal B_1^+ of 30 μT, or 18 μT.

Since we expect a small CEST effect from the amide protons in the healthy glandular tissue, signal stability must be adequate to discern CEST effects from the background noise. Effective lipid suppression is seen with the 1-2-1 binominal excitation pulse (Fig. 2a-c). In addition Fig. 2d-e shows that ghosting levels (Fig. 2d) are below the noise floor (Fig. 2e) when using 30 dummy scans prior to image acquisition. Using the sequence employed in the human volunteers, the CEST results in the creatine phantom (Fig. 3) show a well-resolved CEST effect (Fig. 3a) with a residual peak at approximately 2 ppm offset from the water resonance (Fig 3b). Apart from a substantial residual at the water resonance, the rest of the residual spectrum remained less than 1%.

Three-dimensional, fat-suppressed MR images acquired with an isotropic resolution of 0.6 mm are shown for four volunteers in Figure 4. The average SNR obtained in the indicated circles is 31 ± 4 and varies predominantly in the anterior-posterior direction. In addition, excellent fat suppression is obtained over the entire breast despite the presence of large B_0 and B_1^+ variations. Note that although the density and distribution of glandular tissue varies strongly between the subjects (see for instance subject one with a low dense breast compared to subject 3 with a high dense breast), excellent fat suppression was achieved in all cases.

The overall *z*-spectrum, residual spectrum, and MTR_{asym} averaged over all pixels from glandular tissue are shown in Figure 5. Examination of the residual spectra (Fig 5b) shows a clear residual not only at the APT chemical shift regime of 3.5 ppm, but also at −3.5 ppm, which had been attributed to NOE [10]. The asymmetry between downfield and upfield saturation effects demonstrates a 1% difference (3.5 ppm versus −3.5 ppm). The average APT-CEST fraction from all pixels in glandular tissue for each volunteer was 4% ± 1%, which included a contribution of MT (MT'). Compared to a different cohort imaged at 3 T [9], the standard deviation of these APT-CEST residuals is 4-fold less (Fig. 6a) and the mean value was slightly lower (1% lower). Note that at 3 T a different RF coil was used (16 channel), the spatial resolution was $2.5 \times 2.5 \times 5$ mm^3, the spectral range was −6 ppm to 6 ppm, irradiation was over 1 s, and the total scan time was 6 min and 42 sec. Over the slices that are positioned in the anterior-posterior direction (i.e., the direction of largest B_1+ deviation ranging from 70% to 140% of the nominal B_1^+ setting), no substantial difference in APT-CEST fraction was observed (Fig 6b).

Discussion and conclusion

In this effort, we have demonstrated that high quality saturation spectra including APT-CEST and MT can be reliably obtained in the breast at 7 T. While significant APT effects have been reported at 7 T in human tumors, these data have only been obtained in the brain [7]. Recently, APT-CEST has been examined in human breast cancer at lower field strength (3T) and showed that, while APT-CEST was not statistically distinct from healthy tissue, the APT-CEST temporal evolution during neoadjuvant chemotherapy suggests a possible relationship to treatment response [9]. Unfortunately, the variance of these measurements at 3 T was large (i.e., approximately 5%), thereby limiting the ability to discern subtle changes during, for example, first-line therapy. It is well known that the CEST effect should be enhanced at higher field strengths. In addition, high field provides an increase in SNR. Thus, we have presented our initial experiences with CEST imaging of the breast at 7 T and have also shown that there is a four-fold reduction in the variance of the observed APT-CEST-MT' effect compared to previous results obtained at 3 T.

Importantly, the CEST imaging performed in this study utilized a number of optimized steps to enhance signal stability and maximize the available SNR. It should be noted that we used a sensitivity optimized RF coil to survey each breast unilaterally. The sensitivity-optimized RF coil used at 7 T has been shown to improve SNR by a factor of five when compared to a standard RF coil at 3 T [15]. It should also be noted that no SENSE or other acceleration was used, while the TE was kept short (~2 ms) to minimize losses due to T_2* and ghosting from dynamic field variations. Also, as the CEST data depends on establishing a steady-state, we performed 30 dummy scans to assure a consistent steady state signal intensity. Lastly, the Ernst angle was chosen for the area in glandular tissue that had the lowest B_1^+. While the non uniform B1+ effects CEST contrast, the contrast to noise can still remain uniform as described by Stehouwer et al. [19] and indicated by minimal variance of CEST effects over the slices (Fig 5b). Based on the average SNR of 31 in the high-resolution MRI of the breasts, the SNR of the lower-resolution CEST data, excluding potential instability effects, is approximately 500:

$$SNR \bullet pixel\_volume\_difference \bullet \sqrt{acquisition\_time)difference} = \frac{32 \bullet 3 \bullet 3 \bullet 6}{0.6^3}\sqrt{\frac{1.2}{60 \bullet 5}} = 500$$

CEST MRI is sensitive to physiological effects, sequence parameters and inconsistencies. For example, the CEST effect has been shown to be sensitive to the B_1+ field [17]. This is an important fact because the dependency on B_1^+ is different for different exchanging

groups such that an alteration in the B_1^+ may elicit more contrast from slower (or faster) exchanging species. However, depending on the saturation method used, the B_1^+ field dependence can be minimized. For APT-CEST, we are interested in the slowly exchanging amide protons (i.e., $k_{ex} < 300\ s^{-1}$), and it has been previously shown that optimal CEST effects can be obtained at an effective B_1^+ of approximately 1 μT [17]. Interestingly, in our study, the effective nominal B_1^+ was also 1 μT, yet the APT-CEST-MT' effect did not diminish substantially over the slices where B_1^+ levels differed by a factor of two, indicating robustness to B_1^+ inhomogeneity, in agreement with earlier work [21].

One of the known confounding aspects of CEST imaging is that, for most preparations, the CEST effect is contaminated with MT and direct saturation effects. Additionally, there can be resonance overlap of exchanging proton moieties. Thus we chose to focus our attention on minimizing the impact of lipids, motion, and physiological fluctuations on the CEST acquisition, while recognizing that the effect that is observed is small.

It should be pointed out that the method for analysis of the CEST effect utilized in our study was that of a single Lorentzian. Using this method, we observed a similar residual spectra to that of Jones *et al.* [10] where a broad resonance centered at $\Delta_\omega = +3.5$ ppm is opposite, yet slightly larger than the broad resonance centered at $\Delta_\omega = -3.5$ ppm. We expect that the former is a combination of the MT and APT effect, while the latter has been reported to be an NOE exchange phenomena [10]. There are several drawbacks to the Lorentzian fitting procedure. First, the Lorentzian fit seeks to provide a baseline reflective of only the direct saturation spectra, thus the APT-CEST residual does not remove MT effects like the MTR_{asym} method can, especially at higher saturation powers. Additionally, the Lorentzian fit can also be poor near the water resonance as it assumes that the saturation near the water resonance is driven only by direct saturation, when we know that the CEST spectra near the water resonance results from a combination of both rapidly exchanging hydroxyl protons [5] and direct saturation effects *in vivo*. Using lower saturation powers may reduce the effects of MT and rapidly exchanging hydroxyl protons [10].

While the Lorentzian method has some limitations, it is important to mention its virtues as well. In the case of breast imaging, asymmetry measures are often confounded by not only NOE effects, but also from lipid contamination. In our study, we were able to minimize the impact of fat using a 1-2-1 binomial pulse. Examination of Figure 5 reveals that, even in the absence of lipid components, a significant baseline offset for all non-APT signals in the MTR_{asym} is present; yet for the Lorentzian fit, a close to zero baseline can be achieved. It is important to note that the quantification of the CEST effect using either Lorentzian or asymmetry measures only results in an approximate estimation of the CEST effect and further studies need to be implemented to examine the impact of contaminants on the observed CEST effect.

The CEST experiment presented herein can likely be further optimized. For breast studies, in order to optimize CEST acquisitions going forward, a sophisticated fit at multiple RF powers would need to be provided where the estimated concentrations and observed exchange rates could be calculated. However, from a pragmatic standpoint, other improvement in quantifying the CEST effect at the APT chemical shift may be feasible at 7 T as well. A possible approach is to employ a recently developed CEST method that isolates the rotational component of exchanging protons, the so- called chemical exchange by rotation transfer (CERT [22]). CERT has the feature of being able to discriminate slow from fast exchanging compounds. Note, however, that while the SNR can be sufficient at 7 T for these techniques, stability may need to be considered. Although the standard deviation is as low as 1%, it is higher than expected given the SNR, suggesting instabilities or physiologic variations. Each acquired 3D imaging set was obtained during a large fraction of the

breathing cycle. The resulting large, dynamic field variations (as large as 0.3 ppm [14, 23]) could yield significant temporally varying ghost levels of similar magnitude to the APT effect. In the data obtained in this study, no navigators [24], field probes [13, 24], nor dynamic shimming [13, 14] were applied, all of which could further improve the stability in APT measurements in the breast at 7 T.

Finally, when comparing our results to those obtained by our group at 3 T, it was noticed that the lower field strength measurements were more variable. Apart from the difference in field strength that can contribute to this variance, spatial resolution, RF coil setup, and irradiation time were also different. At 3 T, a 16 channel bilateral coil setup was used compared to a 2 channel unilateral setup at 7T. Consequently at 3 T, sense acceleration was applied resulting in slightly higher spatial resolution (2.5 mm × 2.5 mm ×.5 mm) compared to 7 T (3 mm × 3 mm × 6 mm). In addition, the irradiation time (1 s) at 3 T was less than used at 7 T (4 s), which does not saturate the spins to 100% even though T_1 is substantially less at 3 T. Finally, a different cohort was studied at 3 T. However, note that the variance between subjects is similar to the variance within subjects, which suggests that the standard deviation is mainly caused by SNR and stability rather than physiologic differences in CEST effects. Apart from this SD difference, the APT-CEST fraction also had a higher mean value compared to our 7 T measurements. It is not expected that the exchange rate or concentration differs as a function of field strength; therefore, these phenomena may be related to the pulse sequence parameters, a sensitivity difference, or a relatively reduced inclusion of MT' effect. We propose that this elevation at lower field may also result from poorer spectral resolution, which may result in a more significant overlap of resonances that could artificially inflate the observed CEST effect. This is an area of active investigation.

In conclusion, APT-CEST imaging can be obtained from glandular tissue in the human breast at 7 T at a high level of precision (4 ± 1%), although contamination from MT is included in this value. Together, this work suggests that it may be possible to use this technique to increase sensitivity and specificity in both diagnostic and prognostic settings.

Acknowledgments

We would like to thank the Dutch scientific foundation (ZonMW-VENI2009-916.10.163), the National Institutes of Health (NCI R01CA138599, NCI R25CA092043, and NCI 1U01CA142565), and the National Institute of Biomedical Imaging and Bioengineering (EB000416) for financial support.

Research funding: ZonMW-VENI2009-916.10.163, NCI R01CA138599, NCI R25CA092043, NCI 1U01CA142565, EB000416

Abbreviations

APT	Amide Proton Transfer
CEST	Chemical Exchange by Saturation Transfer
Glu	Glutamate
SNR	Signal to Noise Ratio
TE	Echo time
TR	Repetition time
AFI	Actual Flip angle Imaging
FFE	Fast Field Echo
CERT	Chemical Exchange by Rotation Transfer

References

1]. Zhou J, Payen JF, Wilson DA, Traystman RJ, van Zijl PC. Using the amide proton signals of intracellular proteins and peptides to detect pH effects in MRI. Nat Med. Aug; 2003 9(8):1085–90. [PubMed: 12872167]

[2]. van Zijl PC, Jones CK, Ren J, Malloy CR, Sherry AD. MRI detection of glycogen in vivo by using chemical exchange saturation transfer imaging (glycoCEST). Proc Natl Acad Sci U S A. Mar 13; 2007 104(11):4359–64. [PubMed: 17360529]

[3]. Kim M, Chan Q, Anthony MP, Cheung KM, Samartzis D, Khong PL. Assessment of glycosaminoglycan distribution in human lumbar intervertebral discs using chemical exchange saturation transfer at 3 T: feasibility and initial experience. NMR Biomed. Nov; 2011 24(9): 1137–44. [PubMed: 21387446]

[4]. Cai K, Haris M, Singh A, Kogan F, Greenberg JH, Hariharan H, Detre JA, Reddy R. Magnetic resonance imaging of glutamate. Nat Med. Jan 22; 2012 18(2):302–6. [PubMed: 22270722]

[5]. Haris M, Cai K, Singh A, Hariharan H, Reddy R. In vivo mapping of brain myoinositol. Neuroimage. Feb 1; 2011 54(3):2079–85. [PubMed: 20951217]

[6]. Haris M, Nanga RP, Singh A, Cai K, Kogan F, Hariharan H, Reddy R. Exchange rates of creatine kinase metabolites: feasibility of imaging creatine by chemical exchange saturation transfer MRI. NMR Biomed. Mar 20.2012

[7]. Zhou J, Lal B, Wilson DA, Laterra J, van Zijl PC. Amide proton transfer (APT) contrast for imaging of brain tumors. Magn Reson Med. Dec; 2003 50(6):1120–6. [PubMed: 14648559]

[8]. Sun PZ, Zhou J, Sun W, Huang J, van Zijl PC. Detection of the ischemic penumbra using pH-weighted MRI. J Cereb Blood Flow Metab. Jun; 2007 27(6):1129–36. [PubMed: 17133226]

[9]. Dula AN, Arlinghaus LR, Dortch RD, Dewey BE, Whisenant JG, Ayers GD, Yankeelov TE, Smith SA. Amide Proton Transfer Imaging of the Breast at 3 T: Establishing Reproducibility and Preliminary Data Assessing Chemotherapy Response. Magn Reson Med. 2012 in press.

[10]. Jones CK, Polders D, Hua J, Zhu H, Hoogduin HJ, Zhou J, Luijten P, van Zijl PC. In vivo three-dimensional whole-brain pulsed steady-state chemical exchange saturation transfer at 7 T. Magn Reson Med. Jun; 2012 67(6):1579–89. [PubMed: 22083645]

[11]. Dula AN, Asche EM, Landman BA, Welch EB, Pawate S, Sriram S, Gore JC, Smith SA. Development of chemical exchange saturation transfer at 7 T. Magn Reson Med. Sep; 2011 66(3):831–8. [PubMed: 21432902]

[12]. Mougin OE, Coxon RC, Pitiot A, Gowland PA. Magnetization transfer phenomenon in the human brain at 7 T. Neuroimage. Jan 1; 2010 49(1):272–81. [PubMed: 19683581]

[13]. van Gelderen P, de Zwart JA, Starewicz P, Hinks RS, Duyn JH. Real-time shimming to compensate for respiration-induced B0 fluctuations. Magn Reson Med. Feb; 2007 57(2):362–8. [PubMed: 17260378]

[14]. Boer VO, van de Bank BL, van Vliet G, Luijten PR, Klomp DW. Direct B0 field monitoring and real-time B0 field updating in the human breast at 7 Tesla. Magn Reson Med. Feb; 2012 67(2): 586–91. [PubMed: 22161736]

[15]. Korteweg MA, Veldhuis WB, Visser F, Luijten PR, Mali WP, van Diest PJ, van den Bosch MA, Klomp DJ. Feasibility of 7 Tesla breast magnetic resonance imaging determination of intrinsic sensitivity and high-resolution magnetic resonance imaging, diffusion-weighted imaging, and (1)H-magnetic resonance spectroscopy of breast cancer patients receiving neoadjuvant therapy. Invest Radiol. Jun; 2011 46(6):370–6. [PubMed: 21317792]

[16]. Klomp DW, van de Bank BL, Raaijmakers A, Korteweg MA, Possanzini C, Boer VO, van de Berg CA, van de Bosch MA, Luijten PR. 31P MRSI and 1H MRS at 7 T: initial results in human breast cancer. NMR Biomed. Dec; 2011 24(10):1337–42. [PubMed: 21433156]

[17]. Zu Z, Li K, Janve VA, Does MD, Gochberg DF. Optimizing pulsed-chemical exchange saturation transfer imaging sequences. Magn Reson Med. Oct; 2011 66(4):1100–8. [PubMed: 21432903]

[18]. Haddadin IS, McIntosh A, Meisamy S, Corum C, Styczynski Snyder AL, Powell NJ, Nelson MT, Yee D, Garwood M, Bolan PJ. Metabolite quantification and high-field MRS in breast cancer. NMR Biomed. Jan; 2009 22(1):65–76. [PubMed: 17957820]

[19]. Stehouwer BL, Klomp DW, Korteweg MA, Verkooijen HM, Luijten PR, Mali WP, van den Bosch MA, Veldhuis WB. 7T versus 3T contrast-enhanced breast Magnetic Resonance Imaging of invasive ductulolobular carcinoma: First clinical experience. Magn Reson Imaging. Oct 30.2012 epub.

[20]. Yarnykh VL. Actual flip-angle imaging in the pulsed steady state: a method for rapid three-dimensional mapping of the transmitted radiofrequency field. Magn Reson Med. Jan; 2007 57(1): 192–200. [PubMed: 17191242]

[21]. van Zijl PC, Yadav NN. Chemical exchange saturation transfer (CEST): what is in a name and what isn't? Magn Reson Med. Apr; 2011 65(4):927–48. [PubMed: 21337419]

[22]. Zu Z, Janve VA, Xu J, Does MD, Gore JC, Gochberg DF. A new method for detecting exchanging amide protons using chemical exchange rotation transfer. Magn Reson Med. Apr 13.2012

[23]. Hancu I, Govenkar A, Lenkinski RE, Lee SK. On shimming approaches in 3T breast MRI. Magn Reson Med. May 3.2012

[24]. Versluis MJ, Sutton BP, de Bruin PW, Börnert P, Webb AG, van Osch MJ. Retrospective image correction in the presence of nonlinear temporal magnetic field changes using multichannel navigator echoes. Magn Reson Med. Feb 23.2012

[25]. Barmet C, De Zanche N, Pruessmann KP. Spatiotemporal magnetic field monitoring for MR. Magn Reson Med. Jul; 2008 60(1):187–97. [PubMed: 18581361]

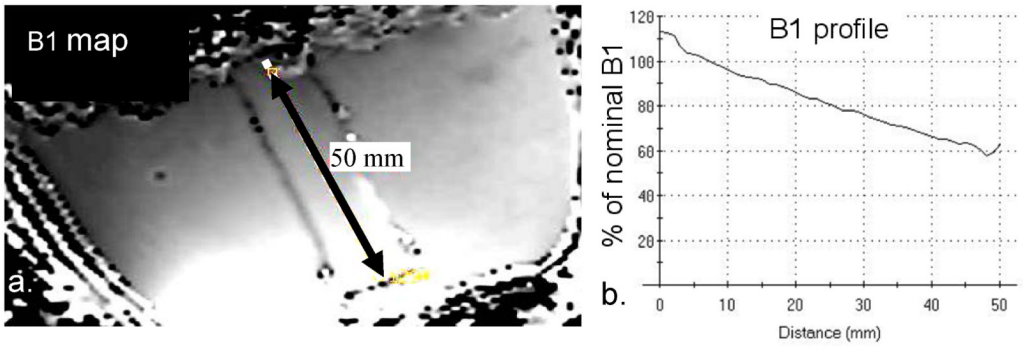

Figure 1.

B1+ map (a) obtained from the phantom at 7T using an RF power setting of 1kW at the coil port for a nominal B1 of 30 μT. Over a range of 5 cm in anterior posterior direction, a 2-fold variance in B1 is observed with an almost linear spatial profile (b).

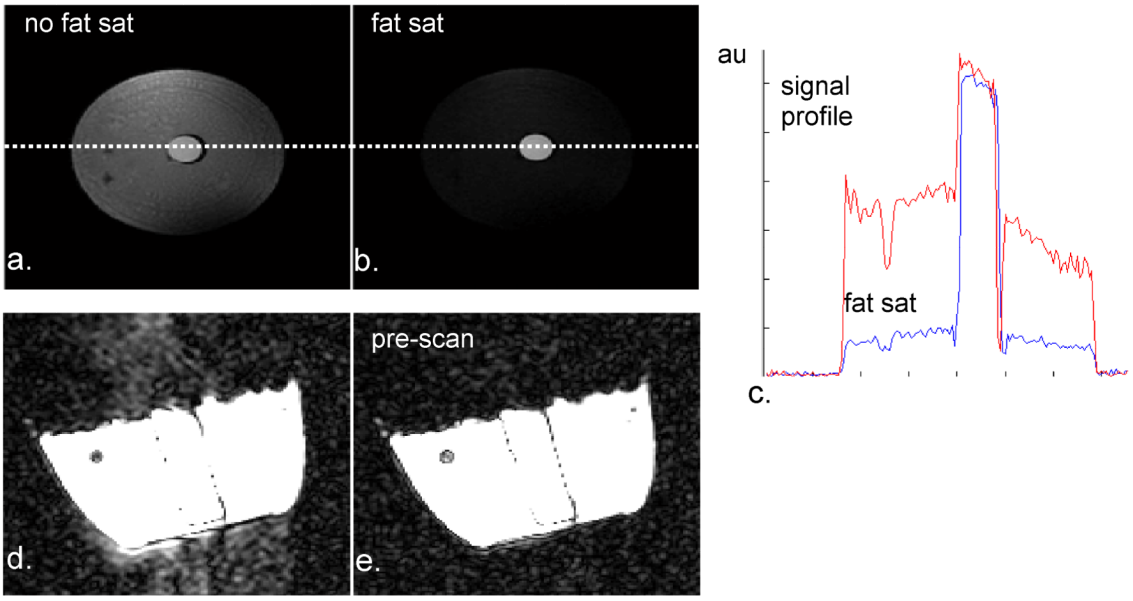

Figure 2.

System performance measurements reflecting effects of lipid suppression and pre-scans in optimizing signal stability. The fat saturation technique of water selective excitation provides a significant reduction of signals from lipid tissue when comparing conventional excitation (a, intensity profile in c) with binominal excitation (b, intensity profile in c). In addition, potential ghosting levels (d) can be reduced even more as reflected by the comparison of 30 additional startup-scans (e) before image acquisition.

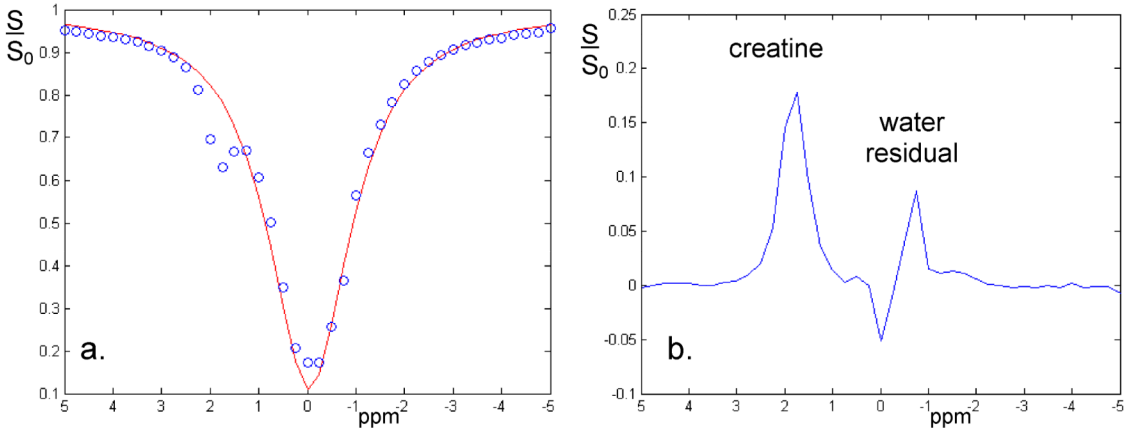

Figure 3.

CEST spectrum obtained from the creatine phantom (a). Using the 10 ms Gaussian-windowed one-lobe sinc 180 degree RF pulses in the saturation train with a sampling interval of 0.25 ppm clearly identifies a CEST effect at about 2 ppm offset from the water resonance (note that the temperature of water was 20 degrees less than in vivo, hence shifting the water resonance position by 0.2 ppm). Subtracting the CEST spectrum from a simple Lorentzian fit (b), normalized to the 1000 ppm offset irradiation data, the creatine peak is fully resolved, while a relatively small residual is observed from directly saturated water.

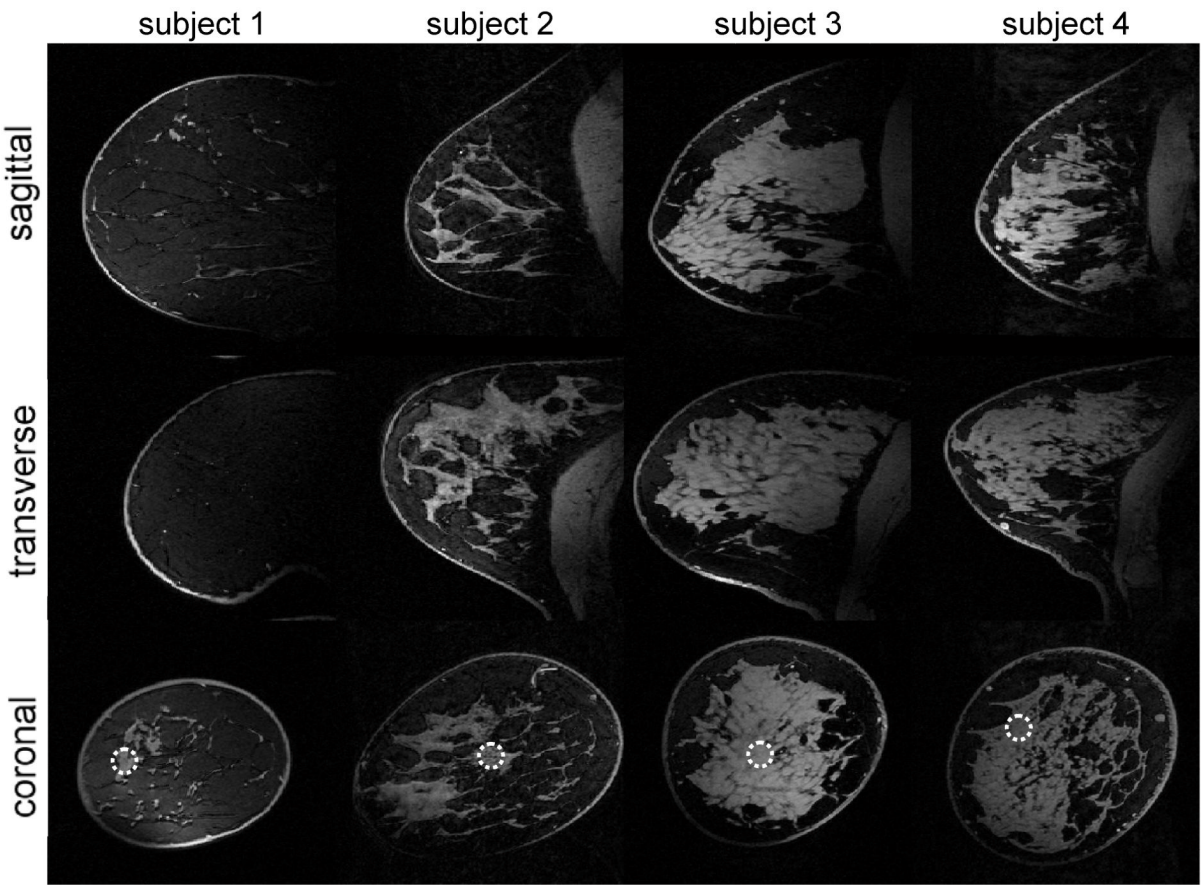

Figure 4.
3D high resolution (0.6 mm isotropic acquired resolution) images obtained from the right breast of healthy volunteers, including fat saturation. Note the relatively uniform pixel intensities of the glandular tissue with a smooth decay in anterior posterior direction. The SNR obtained from glandular tissue at the indicated circles was 37.4, 30.1, 30.8 and 26.6 respectively.

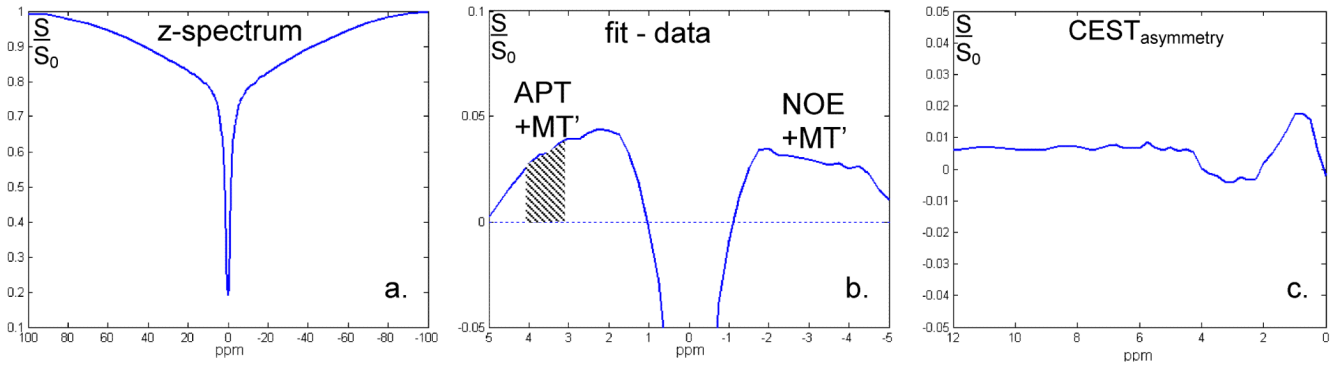

Figure 5.

Results of z-spectrum (a) averaged over the glandular tissue of one subject. After subtraction of the spectrum from its Lorentzian fit (from −5 to 9 ppm), positive signals on both sides of the water resonance can be seen reflecting, apart from a small contribution of MT (MT'), APT (shaded area) and NOE effects respectively (b). The asymmetry with respect to the water resonance is less than 1%, with an observable dip around 3.5 ppm (c). Note though that dynamically changing susceptibility effects during the acquisition of the CEST spectrum can reduce the spectral resolution, the stability of detection remains high as can be observed in the close to 0.1% noise in the CEST asymmetry spectrum (c).

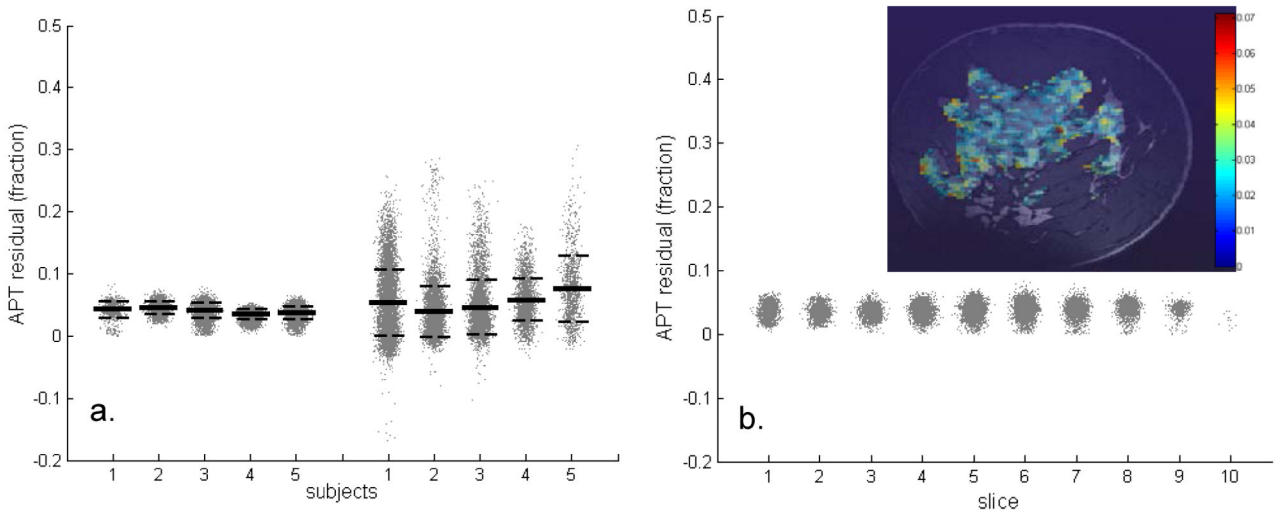

Figure 6.

APT results obtained at 7T from glandular tissue in breasts compared to results obtained at 3T (a) and analyzed for spatial variance (b). A significant reduction in standard deviation (dashed lines) is observed comparing the 7T results (6a, left) to 3T (6b, right), while the average of all fit-residuals at the APT-CEST fraction (lines) remains similar (i.e. 0.04 at 7T and 0.05 at 3T) (a). An example of spatial distribution of APT values within a slice of subject 4 is shown (b, inset). Even between the coronal slices (averaged over all subjects) that each have experienced a different B_1 level, no significant variation in APT effects can be observed (b).